Soft Matter

Cite this: *Soft Matter*, 2011, **7**, 8567

www.rsc.org/softmatter

PAPER

Membrane-mediated interactions between circular particles in the strongly curved regime†

Benedict J. Reynwar‡[a] and Markus Deserno*[ab]

Received 28th February 2011, Accepted 30th May 2011
DOI: 10.1039/c1sm05358b

Particles binding to a fluid lipid membrane can induce bilayer deformations, for instance when these particles are curved. Since the energy of two overlapping warp fields depends on the mutual distance between the two particles creating them, they will experience forces mediated by the curvature of the membrane. If the deformations are sufficiently weak, the associated differential equations for the membrane shape are linear, and the resulting interactions are understood very well; but very little is known for stronger curvature imprint, owing to the highly nonlinear nature of the problem. Here we numerically calculate the magnitude of such membrane-mediated interactions in the case of two axisymmetric particles over a wide range of curvature imprints, deep into the nonlinear regime. We show that over an intermediate distance range the sign of the force reverses beyond a sufficiently strong deformation. These findings are quantitatively confirmed by a simple analytical close-distance expansion. The sign flip can be traced to a change in magnitude between the two principal curvatures midway between the two particles, which can only occur at sufficient particle tilt, a condition which is by construction ruled out in the linearized description. We also show these large perturbation results to agree with coarse-grained molecular dynamics simulations and suggest that a favorable comparison is indeed more likely to hold in the strongly deformed regime.

Introduction

Objects bound to fluid lipid membranes can indirectly interact with each other by means of the curvature deformations they induce in the elastic surface. This phenomenon has been observed experimentally[1] and given rather substantial theoretical reflections.[2–11] In a sufficiently abstract sense it is the old story of particles interacting through fields to which they happen to couple (like charges through the electromagnetic field or masses through space-time), except, maybe, that the field happens to be rather explicitly visible. However, the state of affairs is not quite as drab, because owing largely to the geometric origin of the underlying theory (membrane geometry determines membrane energetics through the Helfrich Hamiltonian[12]), the underlying field equations are highly nonlinear. Membrane-mediated interactions constitute a beautifully explicit and experimentally realizable example of a nonlinear field theory. The flip side is, of course, that it is difficult to work out what the interaction law is. While the analytic implications of stress conservation go a long way,[13–16] quantitative nonlinear force-laws are still only known in one dimension and then require some numerical input.[17–19] And for the arguably most relevant case of particles on two-dimensional membranes, even if they have rotational symmetry, it is not understood how the well-known linear force law[2–5] extends into the regime of strong curvature. Yet, one has every justification to expect fascinating new phenomena: simply recall that exciting gravitational physics exists in the nonlinear (general relativity) regime which is all but absent on the linear (Newtonian) level. For instance, large-scale molecular dynamics simulations suggest that for sufficiently strong axisymmetric curvature imprint membrane-bound particles attract,[20] despite the fact that in the weakly curved linear regime such particles are known to repel.[2–5] Mathematically, this flip of sign in the force law is every bit as striking as if Einstein had discovered that two masses will repel if they are really heavy.

In this paper we study the interaction law between two axisymmetric membrane bending particles through the entire range of imprinted curvature. The nonlinear regime is treated numerically using the package Surface Evolver.[21] We confirm its major findings by a remarkably simple analytical theory, which becomes asymptotically correct at close distances and for curvature imprints near 90°. Most notably, we verify the flip of the sign in the force law, as observed in the simulations, and ascribe it to a subtle crossover phenomenon between different curvature stresses.

[a]*Max-Planck-Institute for Polymer Research, Ackermannweg 10, 55128 Mainz, Germany*
[b]*Carnegie Mellon University, Department of Physics, 5000 Forbes Ave., Pittsburgh, PA, 15213, USA*

† Electronic supplementary information (ESI) available. See DOI: 10.1039/c1sm05358b

‡ Current address: 1629 East Seneca St., Tucson, AZ, USA.

Curvature interactions, the linear case

On the continuum level a deformed fluid lipid membrane is well described by the curvature-elastic energy[12]

$$E = \int \mathrm{d}A \left\{ \sigma + \tfrac{1}{2}\kappa (K - K_0)^2 + \bar{\kappa} K_\mathrm{G} \right\}, \qquad (1)$$

where σ is the surface tension, $K = 1/R_1 + 1/R_2$ the (extrinsic) curvature, $K_\mathrm{G} = 1/(R_1 R_2)$ the Gaussian curvature, R_1 and R_2 are the principal radii of curvature, and where we also have three material parameters, namely the spontaneous curvature K_0, the bending modulus κ, and the saddle splay (or Gaussian) modulus $\bar{\kappa}$. For up-down symmetric membranes $K_0 = 0$. And owing to the Gauss-Bonnet theorem[22,23] the term involving the Gaussian curvature only contributes if either the topology or the boundary of the membrane changes, neither of which will occur in the following. Since, furthermore, we will restrict to tensionless membranes, for which $\sigma = 0$, we can work with the substantially simpler Hamiltonian

$$E = \tfrac{1}{2}\kappa \int \mathrm{d}A \, K^2, \qquad (2)$$

which is proportional to the integrated squared curvature.

In the absence of additional lateral membrane tension the elastic energy of a membrane perturbed by an axisymmetric particle is zero, since the membrane can assume the shape of a catenoid. This axisymmetric minimal surface is a rather special solution of the Helfrich shape equation: by virtue of having zero extrinsic curvature everywhere, $K \equiv 0$, it minimizes the energy density $\frac{1}{2}\kappa K^2$ with its lowest possible value. However, when a membrane contains *two* such particles, no minimal surface solution is possible that satisfies all boundary conditions (*i.e.*, position *and* slope at particle contact). A finite membrane bending energy results that depends on the particle separation r. At zero tension the only other length scale is the particle size a, therefore the interaction energy $U(r)$ between two such particles can only depend on r/a. Within a small gradient approximation one finds[2–5]

$$\frac{U(r)}{\pi\kappa} = 8\,\alpha^2 \left(\frac{a}{r}\right)^4. \qquad (3)$$

Here, α is the contact angle the membrane makes with the plane that contains the particle rim (see Fig. 1). The calculation has been extended to the case of nonzero membrane tension σ by Weikl *et al.*,[5] who showed that the new length scale $\lambda = \sqrt{\kappa/\sigma}$ changes the power law to an exponential. For the case which interests us here, when there is a mirror symmetry plane between the particles, the dominant terms for small a/r and small a/λ are[5]

$$\frac{U(r)}{\pi\kappa} = 2\,\alpha^2 \left\{ \left(\frac{a}{\lambda}\right)^2 \mathrm{K}_0\left(\frac{r}{\lambda}\right) + \left[\left(\frac{a}{\lambda}\right)^2 \mathrm{K}_2\left(\frac{r}{\lambda}\right) \right]^2 \right\}. \qquad (4)$$

In the limit $\sigma \to 0$ (or, equivalently, $\lambda \to \infty$) eqn (4) reduces to eqn (3). Notice that the resulting pair forces are always *repulsive*. Curvature mediated interactions exist, as expected, but they do not lead to an aggregation of particles. Quite on the contrary, they make particles repel each other (at least on the pair level).

These analytical calculations make two main approximations. First, they assume that the membrane is approximately flat and that the distance between the particles is much larger than their size (technically, they result from an expansion in the smallness parameter a/r and, if applicable, a/λ). Second, they are ground-state calculations that neglect membrane shape fluctuations and thus the Casimir interactions also present in these systems. The strength of these fluctuation forces decouples from the ground state terms discussed so far,[8] and thus only depends on the radius a of the particles and not on their curvature imprint α. To lowest order in a/r the associated fluctuation-based potential energy is given by[2,8,24–26]

$$\frac{U(r)}{k_\mathrm{B}T} = -6\left(\frac{a}{r}\right)^4. \qquad (5)$$

Notice that (i) this interaction is *attractive* and (ii) it follows the *same distance dependence* as the (tension free) curvature repulsion. Yet, it is not clear whether it can lead to aggregation of proteins. We see that the fluctuation and the ground state term have a comparable strength for a curvature imprint of $\alpha = (3k_\mathrm{B}T/4\pi\kappa)^{1/2}$, which at a typical value of $\kappa \simeq 20 k_\mathrm{B}T$ amounts to $\alpha \simeq 6^\circ$. Beyond this fairly small curvature the (far-field) ground state repulsion would overwhelm the (far-field) fluctuation induced attraction. Remodeling proteins, which are believed to impose much stronger local deformations (consider for instance the enormous deformation created by a BAR domain[27,28]), should then repel. We hasten to add, though, that a BAR domain imposes a *non-axisymmetric* curvature imprint. In this case even a linear calculation correctly shows that (i) vertical membrane torques align two domains and (ii) aligned domains experience a ground-state attraction with a large distance $1/r^2$ potential.[9] The prefactor of this term vanishes in the axisymmetric limit, thus recovering the isotropic $1/r^4$ repulsion.

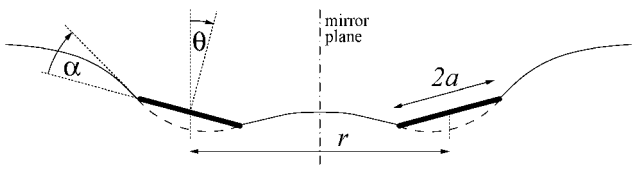

Fig. 1 Cross-sectional schematic of the mirror-symmetric geometry of a pair of membrane deforming proteins. In three dimensions proteins are circular disks of radius a.

Curvature interactions, the nonlinear case

In the present article we use the program "Surface Evolver" of Brakke[21] to calculate – for the first time – the full *nonlinear* curvature-mediated interactions between two axisymmetric particles. We aim to shed light on the following two questions: First, how well does the linear prediction (3) fare for large deformations and/or small separations between the particles? And second, how do results change in the strongly nonlinear regime? Although in this work we focus on

pair-forces, it is worth emphasizing that *multibody effects* in such nonlinear systems can qualitatively change the behavior.[6,29,30] How such effects evolve deep into the nonlinear regime will be important for understanding the aggregation behavior of such membrane proteins, but this is beyond the scope of the present paper.

Methods

Surface Evolver represents a two-dimensional surface embedded in three-dimensional space though an adaptive triangulation and finds the shape that minimizes a given discretized surface Hamiltonian. By adopting the discretized version of (2), we can find the membrane shape that minimizes the Helfrich Hamiltonian for a given set of constraints—which in our case follow from the size, position, and orientation of the membrane-bound circular particles. The patch of membrane considered, when viewed from "above", is a semi-circle with a radius ten thousand times larger than that of the particles (see Fig. 2). The boundary of the membrane is constrained to lie on a semi-circular tube vertically surrounding the semi-circle, and the outward pointing tangent vector of the membrane on that boundary is constrained to be horizontal (notice that the latter does *not* imply that the membrane's unit normal points vertically). One particle lies within this semi-circle and is modeled as a region of membrane that is constrained to lie on a spherical cap. Because we wish to enforce mirror symmetry at the flat side of the semi-circle, the membrane tangent vector perpendicular to this rim is forced to be horizontal. This system is therefore equivalent to two particles centrally located within a much larger circular patch of membrane.

The intersection of the free membrane and the constrained patch that constitutes the model particle is a circle, whose radius a defines the characteristic length scale for our system. We define the position of the particle to be the midpoint of this circle (rather than the center of the sphere which describes the particle's curvature). The separation between the two particles is adjusted by varying the distance between this midpoint and the flat edge of the semi-circular boundary, and the orientation of the particle is altered by tilting this circle around a horizontal axis parallel to the flat edge of the semi circle and passing through its mid point. The angle $\theta = 0$ corresponds to two horizontal particles, whereas $\theta = \frac{\pi}{2}$ corresponds to two particles whose upper surfaces face each other.

For a given set of constraints, Surface Evolver finds the membrane shape that minimizes the energy functional (2), where the integral extends over the entire membrane and all boundary conditions discussed above are required to hold. The triangulation that represents the membrane is refined to different levels in different places depending on the local curvature of the membrane. Briefly, we monitor the dihedral angle between any two triangles, and if this exceeds a predefined maximum, these triangles are further subdivided. To ensure numerical stability the actual procedure used is slightly more complicated and is described in the ESI.† Once the membrane shape minimizing the energy is found, the forces and torques acting on the particle are calculated by measuring the energy change caused by "infinitesimal" translations and rotations. Surface Evolver calculations were performed for (scaled) particle separations r/a ranging from 0.2 to 10, and for contact angles between the particle and the membrane, α, ranging from $\frac{1}{32}\pi \approx 5.6^\circ$ to $\frac{3}{4}\pi = 135^\circ$.

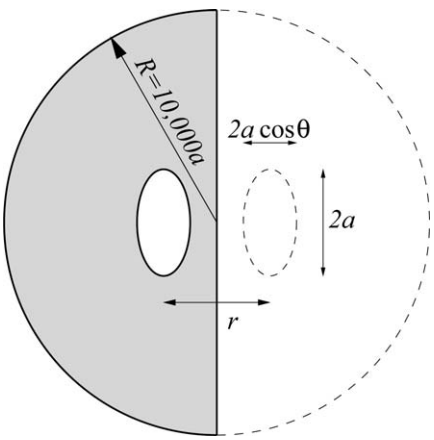

Fig. 2 Schematic top view of the geometry of the Surface Evolver calculation (not to scale). Due to mirror symmetry and horizontal boundary conditions it is sufficient to explicitly represent only the left half of the system. Notice that from above the circular particles appear elliptical at nonzero tilt angle θ.

Numerical results for small curvature imprint

In Fig. 3 we show force–distance-curves for particles with comparatively small membrane contact angles of $\frac{1}{32}\pi$, $\frac{1}{16}\pi$, $\frac{1}{8}\pi$

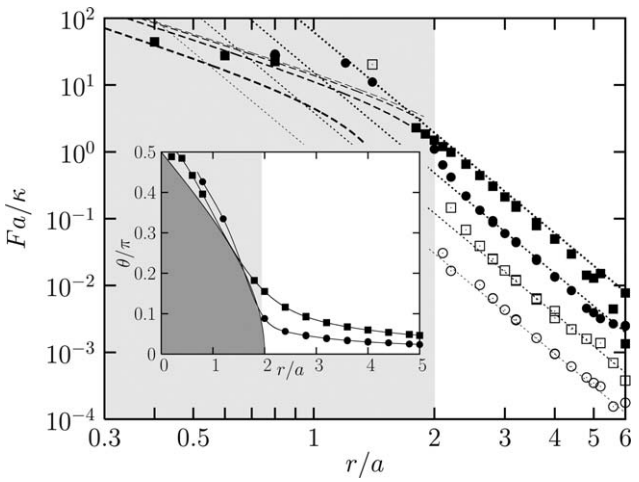

Fig. 3 Force between two weakly curved membrane-bound particles as a function of their separation at different curvature imprint α. The symbols correspond to $\alpha = \frac{1}{32}\pi$ (○), $\frac{1}{16}\pi$ (□), $\frac{1}{8}\pi$ (●), and $\frac{1}{4}\pi$ (■). The dotted lines are the large distance asymptotics from eqn (6). The dashed curves are the small distance asymptotics from eqn (7), with the highest curve corresponding to $\alpha = \frac{1}{32}\pi$ and the lowest to $\alpha = \frac{1}{4}\pi$. The inset shows the rapid rise of the tilt angle θ below $r/a \simeq 2$ for curvature imprints $\frac{1}{8}\pi$ (●) and $\frac{1}{4}\pi$ (■). The distances in the lightly shaded regions are only possible if the particles tilt; the darkly shaded region in the inset ($\theta < \arccos\frac{r}{2a}$) is forbidden.

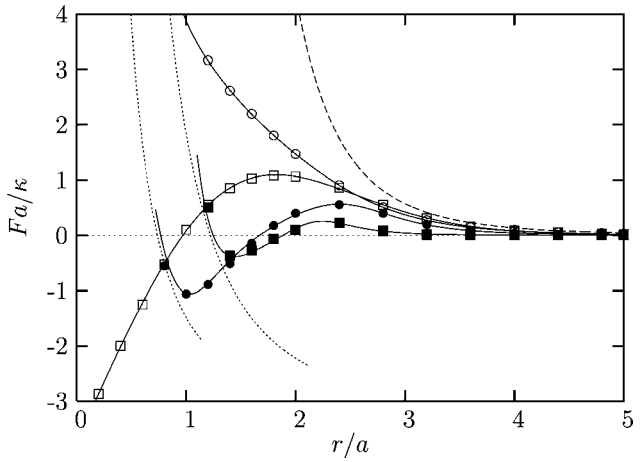

Fig. 4 Force between particles as function of separation. Curves are shown for particles with contact angles of $\frac{3\pi}{8}$ (○), $\frac{\pi}{2}$ (□), $\frac{5\pi}{8}$ (●), and $\frac{3\pi}{4}$ (■). Solid lines are merely guides to the eye. The dashed line is the large-distance analytical prediction for $\alpha = \frac{3\pi}{8}$, while the two dotted curves are the small distance asymptotics from eqn (7b) for contact angles $\frac{5\pi}{8}$ (●), and $\frac{3\pi}{4}$ (■).

and $\frac{1}{4}\pi$. The dotted straight lines correspond to the curvature-mediated force implied by eqn (3),

$$\frac{Fa}{\pi\kappa} = 32\,\alpha^2\left(\frac{a}{r}\right)^5. \qquad (6)$$

As expected, the agreement between the analytical theory and the numerical calculations is very good for large particle separations and small contact angles. However, we confess ourselves astounded by the amazingly good description that the linear far-field theory gives down to separations of $r/a \simeq 2$. This is where the particles – if they were to remain horizontal – would actually *touch*! Also, the full solution agrees remarkably well with the linear calculation for contact angles as large as $\frac{1}{4}\pi = 45°$, even though accuracy clearly diminishes in that case. We found that even though particles with contact angles larger than $\frac{\pi}{4}$ still show the r^{-5} force scaling at large separations, the *prefactors* are smaller than those predicted by eqn (6). The onset of this behavior can be seen in Fig. 3, where the points for $\alpha = \frac{\pi}{4}$ lie noticeably below the analytical prediction.

For separations smaller than $r/a = 2$ the agreement suddenly breaks down quite dramatically. The required tilt θ has to rise very rapidly, since the collision constraint $\theta \geq \arccos\frac{r}{2a}$ must hold (see darkly shaded region in the inset of Fig. 3). Indeed, the tilt rises rapidly, and even though it hardly exceeds the minimum value required by the collision constraint (a remarkable finding in its own right), this soon defeats the small gradient approximation on which the linear theory leading to eqn (6) rests. As a consequence, the forces for small separations are qualitatively different from the predictions. They also vary less as a function of both separation and α. Unfortunately we were not able to calculate very many data points at these short distances, because the associated numerics turned out to be very unstable.

Numerical results for large curvature imprint

Upon slowly increasing the curvature imprint, analytical theory (outside the near-field regime) fails at first only in terms of prefactors. However, beyond a sufficiently large contact angle α qualitatively new effects arise, as can be seen in Fig. 4.§ The force–distance curve for $\alpha = \frac{3\pi}{8}$ still looks similar to that observed for smaller contact angles, in that the repulsion increases continuously at decreasing separation, even though for distances below $r/a \simeq 2.5$ it falls very substantially below the linear prediction. But at the contact angle $\alpha = \frac{\pi}{2}$ we find a fundamentally different functional form of the force law: As the separation is decreased, the repulsive force first increases to a maximum at a separation of $r/a \simeq 1.8$, after which it decreases and at a separation of around $r/a \simeq 1$ becomes *attractive*. This attraction continues to strengthen down to the smallest separation we measured, $r/a = 0.2$. Snapshots of the membrane shape for this contact angle can be seen in Fig. 5 at scaled particle separations $r/a = 0.2$, 2, and 6.

For $\alpha > \frac{\pi}{2}$ a small distance repulsion reappears, so the regime of attractive forces occurs between a minimal and a maximal separation. Of the two stationary points where the force vanishes, the one at the smaller separation is a minimum in the potential, showing that under these conditions two particles can

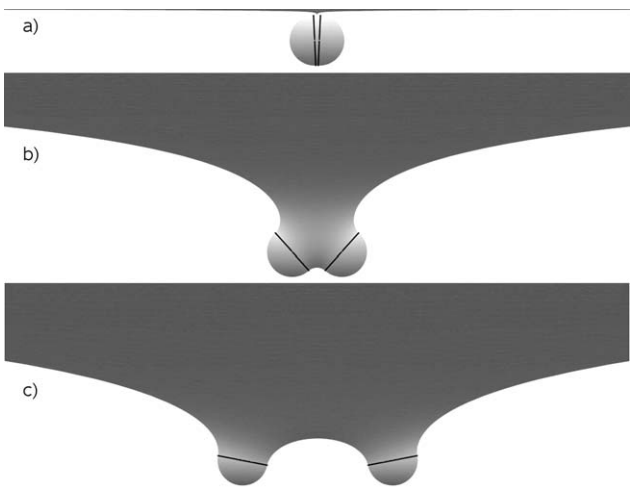

Fig. 5 Images of two membrane-bound particles with contact angles of $\frac{\pi}{2}$ at the zero torque condition. Their separations are (a) 0.2*a*, (b) 2.0*a* and (c) 6.0*a*.

§ The reader might worry whether situations in which α approaches π are physically stable against complete budding or fission. It turns out that a curvature elastic membrane behaves differently than a surface subject to surface tension only, which indeed is unstable against many topology changing events—think of droplets pinching off, or the famous Goldschmidt instability, where a soap film spanned between to coaxial parallel circles of radius *R* collapses once the separation between the circles exceeds $1.32549R$.[31] In contrast, curvature elastic surfaces are stable against such events, which is for instance why on can pull long membrane tethers. Moreover, at any value of α (with or without lateral tension) one can find equilibrium solutions of the shape equation;[32,33] a striking illustration for α close to π is the accumulation of almost completely wrapped but budding-arrested viruses on the surface of cells, as illustrated in the beautiful electron micrographs in the paper by Gottwein *et al.*[34]

(meta-)stably remain at a nonzero distance *without* touching each other.

While the case $\alpha = \frac{\pi}{2}$ is the smallest angle we have studied for which we found attractive forces, continuity considerations strongly suggest that the first instance of an attractive force is reached for some critical value of α smaller than $\frac{\pi}{2}$ but bigger than $\frac{3\pi}{8}$. In fact, a closer study of the small distance behavior for $\alpha = \frac{3\pi}{8}$ suggests the existence of a small non-monotonic "wiggle" (which would be the onset for such a behavior), but we were unable to calculate sufficiently many points to fully verify this.

Analytical theory for small separation

The shape of the membrane for $\alpha = \frac{\pi}{2}$ and $r/a \to 0$, as illustrated in Fig. 5a, essentially extends between the two particles as a circular cylinder, while the rest of the membrane is connected to this structure through a very small catenoidal neck. Making use of the relation $\lim_{r\to 0}\theta(r) = \frac{\pi}{2}$, which is enforced by $\arccos\frac{r}{2a} \leq \theta \leq \frac{\pi}{2}$ (see again the inset of Fig. 3), we therefore propose the following *small distance asymptotics* for the highly nonlinear regime of large tilt.

Consider a contact angle α (not too far away from $\frac{\pi}{2}$) and two close and parallel circular discs, between which the connecting membrane will span. Its shape will be well represented by a toroidal rim of small (signed) curvature radius $c_\perp^{-1} = \rho = r/(2\cos\alpha)$ and large curvature radius $c_\parallel^{-1} = a + \delta = a + \rho(1 - \sin\alpha)$, as sketched in Fig. 6. We assume that the connection to the asymptotically flat parent membrane proceeds indeed *via* a catenoidal neck whose energy will vanish in the limit $r \to 0$, so that we can neglect it altogether in our subsequent discussion.

What is the force transmitted between the two discs through this toroidal bridge? This can be calculated very efficiently by making use of the concept of a *membrane stress tensor*. Briefly, in complete analogy to the notion of stress in deformed solids, one can define a stress tensor for deformed curvature-elastic membranes.[13,35] This tensor gives the *force per length* that acts across a fictitious cut of the membrane along any chosen cutting direction. If this direction coincides with a principal curvature direction (*i.e.*, if it is a local line of curvature), then the answer is very simple: there exists an *attractive* force per length proportional to $\frac{1}{2}\kappa c_\parallel^2$, where $c_\parallel$ is the curvature *parallel* to the cut, and a *repulsive* force per unit length of $\frac{1}{2}\kappa c_\perp^2$, where $c_\perp$ is the curvature *perpendicular* to that cut. If we wish to know the force transmitted through the membrane between the two discs, we merely have to integrate the stress tensor along the circular cross-section of length $2\pi(a + \delta)$ lying half-way between the discs. The symmetry guarantees that this is a line of curvature, and hence we find that the force F mediated between the two particles by the curvature-elastic membrane is given by the expression

$$\begin{aligned}\frac{Fa}{\pi\kappa} &= \frac{a}{\pi\kappa}\times\frac{1}{2}\kappa\left[c_\perp^2 - c_\parallel^2\right]\times 2\pi(a+\delta)\\ &= \frac{a}{\pi\kappa}\times\frac{1}{2}\kappa\left[\left(\frac{1}{\rho}\right)^2 - \left(\frac{1}{a+\delta}\right)^2\right]\times 2\pi(a+\delta)\end{aligned} \tag{7a}$$

$$\begin{aligned}&= \frac{1 + x\,(1-\sin\alpha)}{x^2} - \frac{1}{1 + x\,(1-\sin\alpha)}\\ &= x^{-2} + (1-\sin\alpha)\,x^{-1} - 1 + o(x),\end{aligned} \tag{7b}$$

where we used the scaled distance variable $x = r/(2a\cos\alpha)$. This asymptotic force–distance relation turns out to describe many features of the interaction law in the strongly nonlinear regime. We will now discuss them in detail.

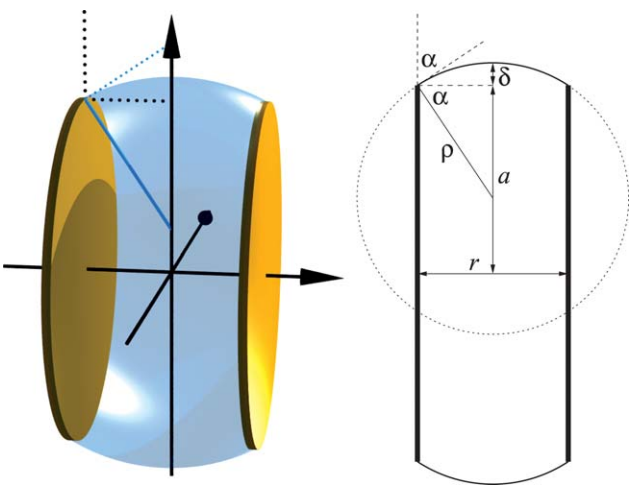

Fig. 6 In the limit where the two circular discs approach very closely, they become essentially parallel, and the membrane assumes the shape of an axisymmetric, "bulged out" cylinder between them. This surface, which is part of a torus, is itself connected to the asymptotically flat membrane by a thin catenoidal neck that is not shown for clarity (but see Fig. 5a). The left three-dimensional graphic illustrates this geometry, the right sketch denotes the variables needed for the analytical calculation underlying this simple shape ansatz.

Discussion

The predictions of the simple analytical model from the previous section are also included in the force–distance plots displayed in Fig. 3 and 4, and we refer the reader to these illustrations while discussing several interesting features worth pointing out explicitly.

1. The functional form of eqn (7b) is very different from the linear result in eqn (6), thus mirroring the observation that for close distances or large angles the linear result is qualitatively off.

2. For small separations eqn (7b) predicts a power-law divergence, but with a much smaller exponent -2, compared to the large distance exponent -5. This explains why the (admittedly sparse) numerical data in the small distance regime in Fig. 3 exhibit a much weaker distance dependence.

3. The dependence of interaction strength on contact angle reverses qualitatively compared to the large distance asymptotics: While for large distances the force becomes stronger with larger angle ($F \propto \alpha^2$), the close distance force becomes *smaller* with increasing angle ($F \propto \cos^2\alpha$), as long as $\alpha \leq \frac{\pi}{2}$. This, unfortunately, cannot be backed up with the few data points we have in this regime.

4. For $\alpha = \frac{\pi}{2}$ we have $\cos\alpha = 0$, hence $x^{-1} = 0$. In this case the particles do not experience a diverging power-law repulsion. Instead, they feel an *attraction* of asymptotic strength $F = \pi\kappa/a$. This is exactly the force transmitted through a cylindrical membrane tube in the absence of tension and area constraints.

Notice that this removal of close distance repulsion happens *only* for $\alpha = \frac{\pi}{2}$.

5. To continue: the prediction $\lim_{r\to 0} F(r)a/\pi\kappa = -1$ and the numerical data are only semi-quantitatively compatible: The smooth extrapolation performed in Fig. 4 does not appear to approach the value $-\pi$. There are two possible reasons for this: First, one needs to bear in mind that the value -1 is the *third* term in an expansion of which the first two vanish for $\alpha = \frac{\pi}{2}$, and it is not clear whether this simple ansatz for the shape is accurate up to third order. In fact, it seems quite remarkable to us that the naïve prediction fares so well. And second, the numerical calculation close to the critical limit $r \to 0$ is especially prone to discretization errors.

6. As eqn (7a) shows, it is the difference between the squared curvature along the line connecting the particles and the squared curvature within the mirror plane which determines the sign of the force. The former needs to become small for the latter to take over. However, the former can only become small if the tilt angle gets close to $\frac{\pi}{2}$. Since linear theory by construction is restricted to small tilts, this partly explains why linear theory invariably predicts a repulsion.

7. For angles α close to $\frac{\pi}{2}$ a stable bound state must exist in which the attractive and repulsive contributions balance. Setting $F = 0$ and using the first three terms in eqn (7b) we see that this leads to a binding distance $r_{\min}$ of

$$\frac{r_{\min}}{a} \simeq \cos\alpha\left(1 - \sin\alpha \pm \sqrt{5 - \sin\alpha(2 - \sin\alpha)}\right), \qquad (8)$$

where the " + " sign holds for $0 \le \alpha \le \frac{\pi}{2}$ and the " − " sign for $\frac{\pi}{2} \le \alpha \le \pi$. For α close to $\frac{\pi}{2}$ this simplifies to $\frac{r_{\min}}{a} \approx 2\,|\alpha - \frac{\pi}{2}|$. We will see soon that this bound state can at most be metastable to the separated state. Notice also that this strongly suggests that attractive interactions also exist for contact angles α somewhat smaller than $\frac{\pi}{2}$, even though we have no explicit force–distance curve to support this conjecture.

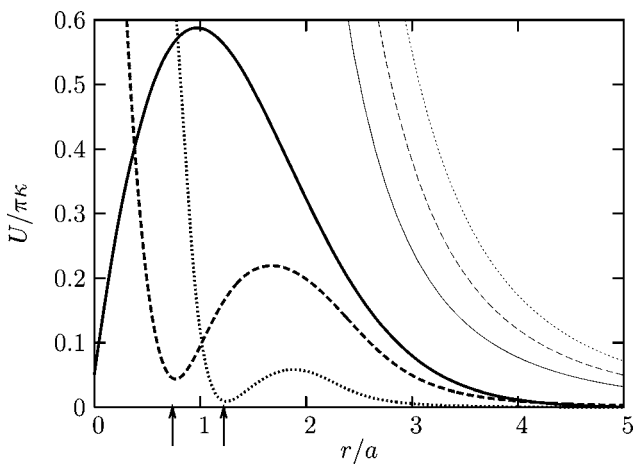

Fig. 7 Potential between particles as function of separation. Curves are shown for particles with contact angles of $\frac{\pi}{2}$ (solid), $\frac{5\pi}{8}$ (dashed), and $\frac{3\pi}{4}$ (dotted). The bold curves are the full nonlinear solution, obtained by numerically integrating the empirical fits to the data in Fig. 4. The fine curves are the linear solution from eqn (3). The two arrows mark the locations of the potential minima in the dashed and dotted case predicted by eqn (8).

Having discussed forces, it would also be instructive to study the associated potentials. One might think it would suffice to merely plot the minimized energy which Surface Evolver yields, but this turns out to be much too inaccurate. The reason is that at different distances Surface Evolver converges to different triangulations, and the associated numerical noise is unfortunately comparable to the energy difference we aim to identify. This is why we instead calculated forces from "virtual" displacements, since these are not nearly as sensitive to the triangulation-dependent numerical noise in the energy. In order to get the potential, we therefore used suitably chosen functions, fit them to the force data as best we could, and then numerically integrated these functions. The results are shown in Fig. 7 for $\alpha \in \{\frac{1}{2}\pi, \frac{5}{8}\pi, \frac{3}{4}\pi\}$. Again, several comments are in order:

1. Since for $\alpha = \frac{\pi}{2}$ and $r \to 0$ the membrane between the particles reduces to a vanishing cylindrical ring and a catenoid of vanishing energy (see again Fig. 5), we expect $\lim_{r\to 0} U(r) = 0$. The deviation of $0.05\pi\kappa$ found in Fig. 7 can thus be taken as some approximate estimate for the error of this procedure to obtain the potential.

2. The functional (2) is positive (semi-)definite; Since the elastic energy imposed by a single particle vanishes (the catenoid – again) and $\lim_{r\to\infty} U(r) = 0$ by conventional choice, the potential energy also satisfies $U(r) = E_{\text{two particles}}(r) - 2E_{\text{one particle}} \ge 0$ at all distances.

3. The nonlinear potentials are all substantially weaker than the linear prediction.

4. As we found when studying forces, metastable minima are possible. In the two cases the prediction for their location from eqn (8) is found to be excellent.

5. Since $U(r) \ge 0$, it is impossible for a close-distance minimum to be more stable than the unbound state, which has $U(\infty) = 0$.

6. Within our accuracy the height of these minima could actually be zero. However, this cannot be generally true, for the following reason: For α close to zero we know that the potential is given by eqn (3), which is a monotonically decaying function. For $\alpha = \frac{\pi}{2}$ it is the solid curve in Fig. 7. For α slightly *smaller* than $\frac{\pi}{2}$ it will qualitatively look similar to the dashed curve (which has $\alpha = \frac{5}{8}\pi$). However, upon continuously increasing α from small values, there is no way to turn a monotonically decreasing function into a positive non-monotonic function which has a minimum that touches zero. Stated differently, the only way to continuously eliminate that minimum at finite distance is to lift it up until the "wiggle" disappears; the alternative of reducing the barrier to zero cannot be true because otherwise the potential would have to be identically zero beyond the finite-distance minimum—which is contradicted by the monotonically decaying small gradient result (3). The fact that these minima seem only metastable with respect to the unbound state is thus real.

7. The barriers particles need to overcome in order to fall into the metastable minima are remarkably small. Assuming $\kappa \simeq 20k_BT$, we find a barrier height of about $13k_BT$ for $\alpha = \frac{5}{8}\pi$ and $4k_BT$ for $\alpha = \frac{3}{4}\pi$.

8. Given the strong reduction of the repulsive force, one might wonder whether the Casimir attraction now becomes competitive. However, for $r/a = 2$, $\alpha = \frac{3}{4}\pi$, and again $\kappa \simeq 20k_BT$, we have

$$\frac{U_{\text{Casimir}}(2a)}{U_{\text{ground state}}(2a)} \simeq \frac{6\,k_B T\,2^{-4}}{4\,k_B T} \approx 0.1, \tag{9}$$

which leaves U_{Casimir} about an order of magnitude smaller than the remaining barrier for $\alpha = \frac{3}{4}\pi$. Of course, the magnitude of the fluctuation forces will be quite different at such a large deformation, so this estimate must be taken with more than just a grain of salt. But it nevertheless gently reminds us that there is no *obvious* reason to expect fluctuations to dominate over the ground state at large curvature imprint (even though of course they might end up doing just that).

Comparison with coarse-grained molecular dynamics simulations

We have previously studied the forces between curvature-imprinting particles[20] through coarse-grained (CG) Molecular Dynamics simulations using the ESPResSo[36] package. Details of the implementation can be found in this earlier paper and its accompanying supplementary material. We briefly summarize the facts which matter for the following discussion:

We examined particles constructed as hollow spheres and inflated by filler particles to reach a bare radius $R_0 \simeq 5.5\sigma$ (with the CG length σ mapping roughly to 1 nm) and $\alpha = \frac{2}{3}\pi$ (implemented by a strong difference in adhesion energy between sphere surface and lipid head group). We defined the effective radius R relevant for membrane bending to be the physical radius of the capsid, R_0, plus half the thickness of the membrane, $d \simeq 6\sigma$, for a total of $R = R_0 + \frac{1}{2}d = 8.5\sigma$. The particles were placed on a square patch of membrane (using the Cooke model[37,38]) containing 10 240 lipids and having initial dimension of $80\sigma \times 80\sigma$. A modified Andersen barostat[39] kept the tension in both x and y direction at zero by adjusting the box-length to compensate for any nonzero stress. The spheres were placed with a line of connection parallel to the y direction. Their center-to-center distance was constrained to d_c, but they could still move vertically and rotate. Notice that this sphere-based way of specifying the geometry slightly differs from the disc-based one discussed so far. However, it is quite easy to see that these two descriptions are related by

$$\frac{d_c}{R} = \frac{r}{a}\sin\alpha - 2\cos\alpha\sin\theta. \tag{10}$$

A cross-section of a typical configuration is illustrated in the inset of Fig. 8.

The filled squares in Fig. 8 are the membrane-mediated forces between these particles as measured earlier,[20] determined from the constraint force necessary to fix the particle separation to d_c. At short distances the particles repel strongly, at larger distances a substantial attraction exists that persisted to the largest values of d_c we examined. While the data do not tell how it develops beyond $d_c/R = 2.5$, an attraction extending to infinity is not possible within a bending-only ground state framework, as explained above, but it is conceivable that other effects (fluctuations, lipid packing and protrusions, tilt fields, *etc.*) complicate matters.

To study this further, we performed additional simulations to explore larger separations, but also refined our setup:

1. We used a membrane containing twice as many lipids, extending twice as far in the x-direction. Exact analytical theory shows that the force is fully determined by a line integral over geometric membrane properties on the intersection curve between the membrane and the mirror plane,[15,16] and since deformations of this curve extend quite far away from the capsids, we want to avoid a premature cutoff.

2. Since the barostat involves changes in the box length, this can interfere with the distance constraint of the particles along the y-direction. Hence we decided this time to only adjust the box length in x-direction.

3. Besides the old way of constructing the particles we also used a second strategy, in which capsids are modeled as rigid but hollow spheres, in which suitable bending potentials support the spherical geometry. These spheres have the same size, amphiphilic surface structure, and attraction strength in the adhesive region as the hollow spheres (notice that the "filler beads" never attracted the lipids). We will refer to the former construction as "filled spheres" and the new one as "hollow spheres". In both cases the spheres deformed negligibly during the simulation.

The circular symbols in Fig. 8 correspond to our new simulation data, which add the following information:

1. The overall functional force–distance relation is compatible with the continuum prediction from Fig. 4. We have no simulations which exactly match the continuum calculations in terms of contact angle, and in fact the precise value of that angle is difficult to unambiguously define in the simulation due to discreteness issues. However, the case $\alpha = \frac{2}{3}\pi$ is bracketed between the two continuum curves for $\alpha = \frac{5}{8}\pi$ and $\alpha = \frac{3}{4}\pi$.

2. More specifically, the possibility of an asymptotic attraction seems ruled out. Both curves suggest that for d_c/R somewhere between 2 and 2.5 the attraction reverts back to a repulsion. Since this crossover is predicted to be around $\frac{r}{a} \simeq 1.8$ (see Fig. 4) and in this case the tilt angle is approximately $\theta \simeq \frac{1}{4}\pi$ (see Fig. 5b), we

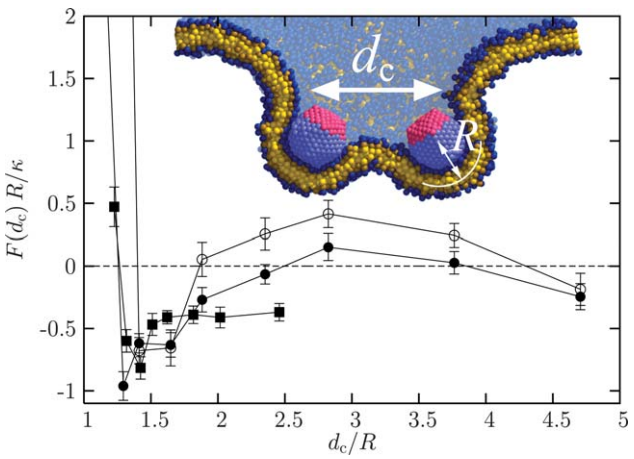

Fig. 8 Forces measured between constrained spherical particles with $\alpha = \frac{2}{3}\pi$ measured in CG Molecular Dynamics simulations. Solid squares (■) are the results presented in an earlier publication,[20] the circular symbols are from this work, in which the membrane has been enlarged, the barostat applied differently, and two different capsid constructions tested: filled spheres (●, as previously) and hollow rigid spheres (○). The inset shows the cross-section of a typical configuration.

find from eqn (10) that $\frac{d_c}{R} \simeq 2.3$ for the crossover predicted in the simulation data, which is indeed compatible with Fig. 8.

3. For the force we find $\frac{Fa}{\kappa} = \frac{FR\sin\alpha}{\kappa} \simeq 0.866\ \frac{FR}{\kappa}$. From Fig. 8 we get $\frac{F_{\max}R}{\kappa} \approx 0.75$ for the maximal attractive force, implying $\frac{F_{\max}a}{\kappa} \approx 0.65$, in line with Fig. 4, when again interpolating between the two angles $\frac{5}{8}\pi$ and $\frac{3}{4}\pi$.

4. Disconcertingly, the two different capsid constructions appear to make a small but statistically significant difference in the forces. We were unable to trace the origin of this effect, but would like to emphasize that it does not affect the general behavior: A large scale repulsion, followed by a medium-range attraction, which ultimately goes into a strong short range repulsion (in the case that the curvature imprint is large enough). While we therefore expect the exciting feature of an intermediate attraction to be universally true, its overall strength might depend on subtle details of the particles involved, which makes it difficult to (i) compare with experiment or simulation and (ii) tune such interactions in experiment, say by suitable surface coatings.

Conclusions and outlook

Taken together, our exact numerical solutions of the shape equations and the CG Molecular Dynamics simulations show that curvature mediated interactions between axisymmetric membrane curving particles display exciting new physics in the strongly nonlinear case of large curvature imprint. While for large distances and weak bending the linear solution fares exceedingly well, it is incapable of predicting the crossover into a regime in which *attractive* forces exist over a range of distances that is bounded both below and above. We have identified these forces both in continuum theory and simulation, with results that are compatible (when accounting for slight differences in geometric definitions). Moreover, a remarkably simple close-distance analytical model can account for almost all novel features of the nonlinear regime, thus further corroborating the novel findings beyond the linear realm.

These studies support the view that the attractive forces between strongly membrane deforming objects, as identified in our earlier simulations,[20] are indeed manifestations of *curvature mediated interactions* and not merely artifacts of various other possible mechanisms that might be operative in the simulation (which is is of course more complex than a simple continuum Helfrich membrane).

Despite the agreement between simulation and theory in this regime, it must be pointed out that a number of mysteries still remain:

1. In the (seemingly less formidable) case of weaker curvature imprint (say, $\alpha \sim \frac{1}{4}\pi$) analytical theory clearly predicts a repulsion over the entire range of distances. And yet, many curvature imprinting disks with α in this range are able to cooperatively drive vesiculation.[20] It is possible that multi-body effects, not discussed in the present work, change the pair-picture.[6,29]

A fascinating scenario along these lines has recently been put forward by Auth and Gompper: Many curvature imprinting proteins can drive vesiculation precisely *because* they repel.[30] The formation of a macroscopically curved membrane that accommodates the protein curvature reduces the repulsion and thus lowers the energy. This requires the confinement of all proteins in a finite area of the membrane, which indeed happens in simulations of finite membrane patches, but which would need to be enforced by other means in a biological context. Laterally segregated domains which preferentially bind the membrane curving proteins could for instance accomplish such a task.

2. The time evolution of budding events driven by many spheres with $\alpha = \frac{2}{3}\pi$ (see Supplementary Video 3 of ref. 20) shows that these spheres readily "fall" towards each other over distances bigger than $d_c/R \simeq 2$, without any indication that an energy barrier of 5…10 k_BT would need to be overcome. Even though Fig. 8 supports the view that the barrier predicted by continuum theory also exists in the simulations, its magnitude cannot be quantified very precisely, because the forces at larger distances become exceedingly small and thus very hard to measure with sufficient accuracy. Recall also that, disconcertingly, the barrier depends sensitively on details (such as the capsid construction protocol) whose relevance is not obvious. A second caveat is that these multi-capsid simulations are not done under exactly the same conditions for which our continuum results have been derived: Apart from the fact that *many* capsids are involved, thereby changing the boundary conditions relevant to this situation, a possibly more severe issue is that the system is *not* in equilibrium (capsids move towards each other), and the overall membrane might simply not have had enough time to adjust to some energy-minimizing shape for which the forces could conceivably be different.

3. For smaller curvature imprint the geometry forces weaken and become comparable to a variety of other membrane mediated interactions, such as tilt mediated forces, lipid packing effects, or fluctuations of any of these mediating fields. Once this happens, the net result is likely a coaction of considerable complexity, and it is unclear how meaningful progress can be obtained through analytical theory. Curiously, the strong curvature regime might thus be conceptually easier than the weak one, if the geometric component dominates the others.

We would like to conclude by reminding the reader that throughout this article we have focused on a very small region of parameter space: that of *inflexible*, *symmetric* particles on a *zero-tension* and *unconstrained* membrane. Yet, even within this small region of parameter space there remain rather fundamental unanswered questions. Further ground-state calculations – possibly going beyond Helfrich theory – as well as calculations that capture the effect of fluctuations more systematically and to higher order are clearly required. Most importantly however, controlled experiments that attempt to isolate these effects between real particles on a real membrane are necessary to give us a guideline that can be used to advance our understanding of these forces. They can easily compete with other more "conventional" interactions between membrane bound particles, and yet we cannot so far describe them as quantitatively as needed in many situations where it would matter.

Acknowledgements

We would like to thank Ken Brakke for his advice on the use of Surface Evolver and Martin Müller for stimulating discussions. MD is grateful for the hospitality of the Theory Department at the MPI-P during a summer sabbatical, where some of this work

has been completed. Financial support from SFB 625 and the German Science Foundation (De775/1-4) is also gratefully acknowledged.

References

1 I. Koltover, J. Rädler and C. Safinya, *Phys. Rev. Lett.*, 1999, **82**, 1991.
2 M. Goulian, R. Bruinsma and P. Pincus, *Europhys. Lett.*, 1993, **22**, 145.
3 M. Goulian, R. Bruinsma and P. Pincus, *Europhys. Lett.*, 1993, **23**, 155.
4 J.-B. Fournier and P. Dommersnes, *Europhys. Lett.*, 1997, **39**, 681.
5 T. Weikl, M. Kozlov and W. Helfrich, *Phys. Rev. E: Stat. Phys., Plasmas, Fluids, Relat. Interdiscip. Top.*, 1998, **57**, 6988.
6 K. Kim, J. Neu and G. Oster, *Biophys. J.*, 1998, **75**, 2274.
7 P. Dommersnes and J.-B. Fournier, *Eur. Phys. J. B*, 1999, **12**, 9.
8 P. Dommersnes and J.-B. Fournier, *Europhys. Lett.*, 1999, **46**, 256.
9 P. Dommersnes and J.-B. Fournier, *Biophys. J.*, 2002, **83**, 2898.
10 D. Bartolo and J.-B. Fournier, *Eur. Phys. J. E*, 2003, **11**, 141.
11 A. Evans, M. Turner and P. Sens, *Phys. Rev. E: Stat. Phys., Plasmas, Fluids, Relat. Interdiscip. Top.*, 2003, **67**, 041907.
12 W. Helfrich, *Z. Naturforsch. C*, 1973, **28**, 693.
13 R. Capovilla and J. Guven, *J. Phys. A: Math. Gen.*, 2002, **35**, 6233–6247.
14 J. Guven, *J. Phys. A: Math. Gen.*, 2004, **37**, L313–L319.
15 M. M. Müller, M. Deserno and J. Guven, *Europhys. Lett.*, 2005, **69**, 482.
16 M. Müller, M. Deserno and J. Guven, *Phys. Rev. E: Stat., Nonlinear, Soft Matter Phys.*, 2005, **72**, 061407.
17 P. Biscari, F. Bisi and R. Rosso, *J. Math. Biol.*, 2002, **45**, 37–56.
18 P. Biscari and F. Bisi, *Eur. Phys. J. E*, 2002, **7**, 381–386.
19 M. M. Müller, M. Deserno and J. Guven, *Phys. Rev. E: Stat., Nonlinear, Soft Matter Phys.*, 2007, **76**, 011921.
20 B. Reynwar, G. Illya, V. Harmandaris, M. Müller, K. Kremer and M. Deserno, *Nature*, 2007, **447**, 461–464.
21 K. Brakke, *Exp. Math.*, 1992, **1**, 141–165.
22 M. Do Carmo, *Differential Geometry of Curves and Surfaces*, Prentice-Hall, Englewood Cliffs, NJ, 1976.
23 E. Kreyszig, *Differential Geometry*, Dover, New York, 1991.
24 R. Golestanian, M. Goulian and M. Kardar, *Phys. Rev. E: Stat. Phys., Plasmas, Fluids, Relat. Interdiscip. Top.*, 1996, **54**, 6725.
25 J. Park and T. Lubensky, *J. Phys. I (Paris)*, 1996, **6**, 1217.
26 W. Helfrich and T. Weikl, *Eur. Phys. J. E: Soft Matter Biol. Phys.*, 2001, **5**, 423–439.
27 B. Blood and G. Voth, *Proc. Natl. Acad. Sci. U. S. A.*, 2006, **103**, 15068.
28 A. Arkhipov, Y. Yin and K. Schulten, *Biophys. J.*, 2008, **95**, 2806–2821.
29 M. Müller and M. Deserno, *Prog. Theor. Phys., Suppl.*, 2010, **184**, 351.
30 T. Auth and G. Gompper, *Phys. Rev. E: Stat., Nonlinear, Soft Matter Phys.*, 2009, **80**, 031901.
31 C. Isenberg, *The Science of Soap Films and Soap Bubbles*, Dover, NewYork, 1992.
32 M. Deserno and T. Bickel, *Europhys. Lett.*, 2003, **62**, 767.
33 M. Deserno, *Phys. Rev. E: Stat., Nonlinear, Soft Matter Phys.*, 2004, **69**, 031903.
34 E. Gottwein, J. Bodem, B. Müller, A. Schmechel, H. Zentgraf and H.-G. Kräusslich, *J. Virol.*, 2003, **77**, 9474.
35 J.-B. Fournier, *Soft Matter*, 2007, **3**, 883–888.
36 H.-J. Limbach, A. Arnold, B. A. Mann and C. Holm, *Comput. Phys. Commun.*, 2006, **174**, 704–727.
37 I. Cooke, K. Kremer and M. Deserno, *Phys. Rev. E: Stat., Nonlinear, Soft Matter Phys.*, 2005, **72**, 011506.
38 I. Cooke and M. Deserno, *J. Chem. Phys.*, 2005, **123**, 224710.
39 A. Kolb and B. Dünweg, *J. Chem. Phys.*, 1999, **111**, 4453–4459.